ACS OMEGA

http://pubs.acs.org/journal/acsodf

Article

Oxidation Resistance Improvement of Graphene-Oxide-Semiconductor Planar-Type Electron Sources Using h-BN as an Oxygen-Resistant, Electron-Transmissive Coating

Naoyuki Matsumoto, Yoshinori Takao, Masayoshi Nagao, and Katsuhisa Murakami*

Cite This: *ACS Omega* 2022, 7, 33004−33009

Read Online

ACCESS | Metrics & More | Article Recommendations

ABSTRACT: Graphene−oxide−semiconductor (GOS) planar-type electron emission devices with a hexagonal boron nitride (h-BN) protective layer have demonstrated improved oxidation resistance while maintaining their emission performance. The devices with a monolayer or a multilayer (13 nm in thickness) h-BN protective layer can emit electrons even after oxygen plasma exposure (ashing). Remarkably, the device with a monolayer h-BN was able to emit electrons with a maximum efficiency of 11% after a 4-min ashing, showing that a thin h-BN protection layer can provide oxygen tolerance to GOS devices without a significant emission loss. The thicker multilayer h-BN imparted higher oxidation resistance to the device but with decreased emission efficiency compared with the device with monolayer h-BN. Thus, the use of h-BN necessitates a trade-off between the device's emission performance and its oxidation resistance. In addition, the etching rate of h-BN by the oxygen plasma treatment was found to increase by exposure to air after the first plasma treatment, which indicates that the adherence of H_2O to the surface of h-BN is one probable cause of h-BN etching during the ashing process.

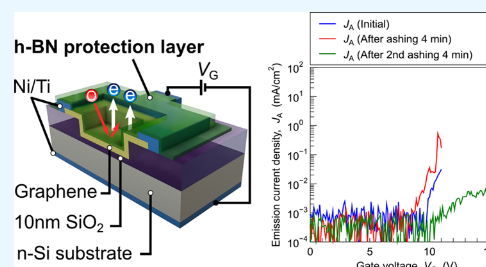

■ INTRODUCTION

Planar-type electron sources like metal−oxide−semiconductor or metal−oxide−metal devices have attractive features, e.g., low drive voltages (<20 V),[1] electron beams with lower divergence angles,[2] and electron emission capability not only in a high vacuum but also in a low vacuum,[3,4] and even in a liquid.[5] In addition, the planar-type electron source based on a graphene−oxide−semiconductor (GOS) structure has achieved high electron emission densities of 1−100 mA/cm^2 with high emission efficiencies of 10−50% by introducing graphene as an electron-transmissive gate electrode.[6−9] Because of these excellent advantages, GOS devices are expected to be used in further applications, such as a neutralizer cathode for miniature ion thrusters mounted on nano/microsatellites flying in low Earth orbit,[10] an electron source for a low-cost and high-resolution scanning electron microscope (SEM) that can be operated in a low-vacuum state,[11,12] and an electron source for a hydrogen evolution reaction in a liquid.[5] These applications require the GOS device to be operable in oxidative environments, e.g., a low Earth orbit where atomic oxygen is the dominant gas component,[13] a low vacuum containing O_2 molecules, and a liquid containing oxygen atoms. However, a concern is that if the GOS device is operated in these environments, the topmost layer of the graphene electrode would be oxidized and removed, resulting in the loss of the device's electron emission capability. Therefore, to realize further applications of the GOS electron source, improving the oxidation resistance while maintaining the device's emission performance is an imperative goal that has not yet been realized.

Hexagonal boron nitride (h-BN), a two-dimensional (2D) layered material composed of boron and nitrogen atoms, is promising as a protective material for graphene electrodes. Using a material with a small atomic number in the protective layer will help to avoid a decrease in the emission current due to inelastic scattering. Because h-BN is composed of atoms that have a small atomic number and are inert to oxygen, this material has a high potential to realize enhancement of oxidation resistance with less performance degradation of the GOS device. Previous studies from other research groups have also demonstrated its high oxidation resistance and[14] its effectiveness as a protective layer against atomic oxygen[15] and high-temperature air.[16,17] In addition, electron inelastic scattering with phonons of h-BN was found to be very small compared to that of SiO_2 from our previous studies of planar-type electron devices based on a graphene/h-BN/n-Si heterostructure, which utilized h-BN layer as the insulating

Received: May 1, 2022
Accepted: August 15, 2022
Published: September 6, 2022

© 2022 The Authors. Published by American Chemical Society

https://doi.org/10.1021/acsomega.2c02709
ACS Omega 2022, 7, 33004−33009

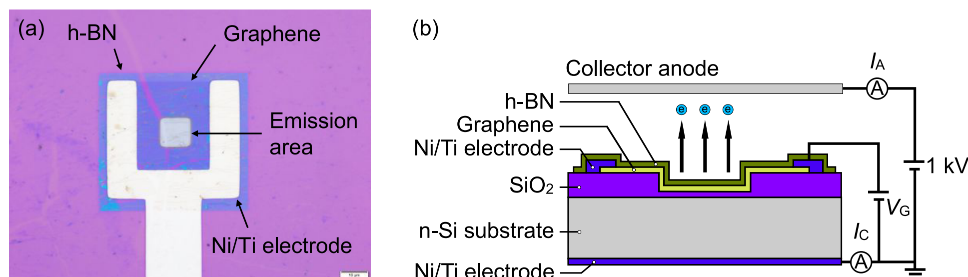

Figure 1. (a) An optical image of GOS with multilayer h-BN and (b) schematic of the emission performance measurement setup.

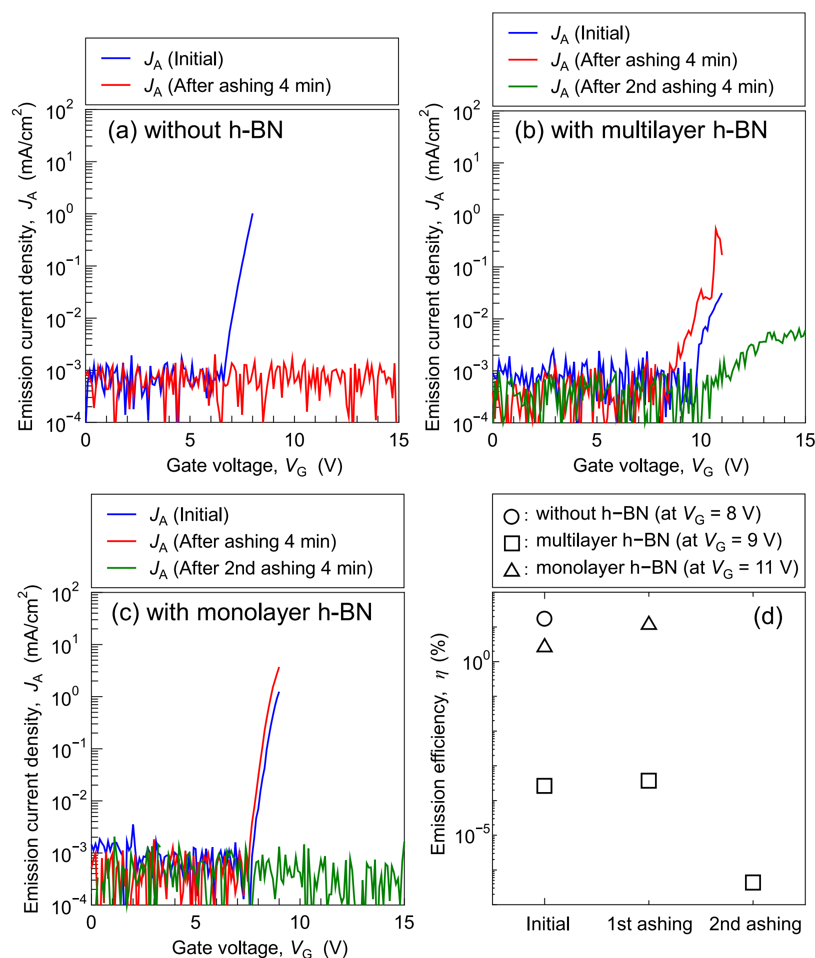

Figure 2. $J_A - V_G$ curves of the GOS device before and after ashing (a) without h-BN, (b) with multilayer h-BN, and (c) with monolayer h-BN. (d) Their emission efficiency.

layer of the GOS devices instead of a conventional SiO_2 insulator.[18,19] This result implies that h-BN has excellent potential as the electron-transmissive layer. Therefore, the high oxidation resistance and electron transmissivity of h-BN suggest its suitability as a protective material for GOS electron sources. However, the potential of h-BN as an oxygen resistance protective layer for GOS electron sources has not been investigated in detail. In this study, we demonstrated the effectiveness of h-BN as the oxygen resistance protection layer of the GOS devices. The dependence of the oxidation resistance and electron emission efficiency of GOS devices on the thickness of h-BN was further investigated.

■ EXPERIMENTAL SECTION

In this study, a GOS device with an h-BN protective layer was fabricated by the following procedure, and its electron emission performance and oxidation resistance were evaluated. Photolithography and wet etching were applied to an n-type Si substrate with a 300 nm thick SiO_2 layer to form a 10 μm square emission area. After the standard semiconductor cleaning method called "RCA standard clean,"[20,21] a thin SiO_2 insulating layer of 10 nm was grown by thermal oxidation at 950 °C under an O_2 flow of 1 L/min at atmospheric pressure. A graphene electrode with a thickness of 1 nm, corresponding to around 3 layers of graphene, was directly deposited by plasma-enhanced chemical vapor deposition (CVD) at 700 °C using methane as a carbon source.[10,18,19]

https://doi.org/10.1021/acsomega.2c02709
ACS Omega 2022, 7, 33004−33009

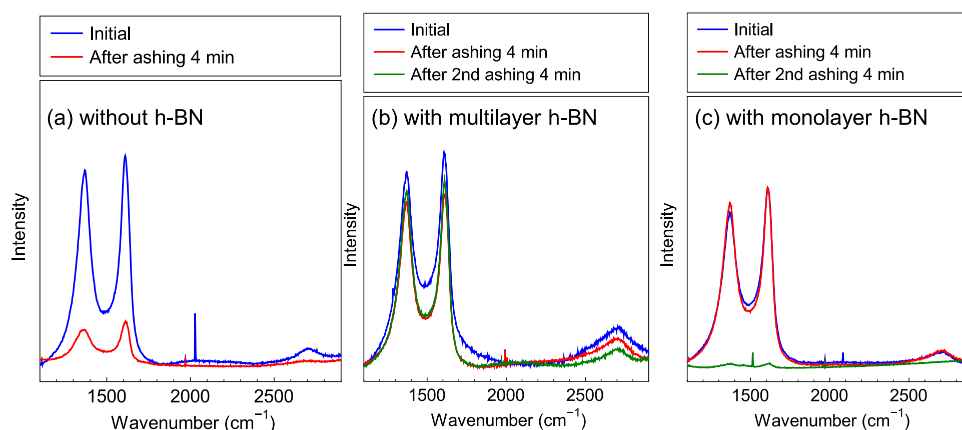

Figure 3. Raman spectra of graphene electrode of the GOS device before and after ashing (a) without h-BN, (b) with multilayer h-BN, and (c) with monolayer h-BN.

After the graphene was partially etched by oxygen plasma, the contact electrodes of Ni (100 nm)/Ti (10 nm) stack were formed by a process of electron beam evaporation and lift-off. Then, the back contact electrode with the same material and thickness as the contact electrode was deposited on the wafer's back surface by electron beam evaporation. Multilayer (13 nm in thickness) or monolayer h-BN films synthesized on Cu foil (EM Japan Co., Ltd., Cat no. G-53 and G-54) were used for the protective layer. The transfer of h-BN onto the graphene electrode from Cu foil was accomplished according to the technique described in ref 18. A small amount of organic residue caused by a photoresist used in the transfer processes remained on the h-BN surface. To evaluate the effect of the h-BN layer and its thickness on the oxidation resistance and emission performance of the GOS device, three types of devices were fabricated: with multilayer h-BN, with monolayer h-BN, and without the h-BN protective layer.

As an oxidation resistance test, all three samples were exposed to an O_2 plasma of 100 W for 4 min using an oxygen plasma asher (referred to as ashing). Before and after ashing, the emission current densities were measured versus the applied gate voltages of the device to evaluate the oxidation resistance. The h-BN surface was exposed to air before and after the ashing process, as the oxygen plasma ashing was conducted ex situ in another chamber after the emission measurements. The Raman spectra of the graphene electrode were also measured to confirm that graphene remains. The cycles of the emission test, Raman spectrometry, and ashing were continued until the GOS devices had lost their capability for electron emission.

■ RESULTS AND DISCUSSION

Figure 1 shows an optical image of the device with multilayer h-BN and a schematic of the measurement setup of the device's emission performance. The h-BN protection layer had several wrinkles and cracks which were generated during the transferring processes of h-BN from the Cu foil. By applying the gate voltage, V_G, electrons are emitted from the emission area; these electrons encounter the 1-kV applied collector anode, and the emission current I_A is measured. The cathode current is measured as I_C, which includes the total current passing through the SiO_2 insulating layer. To evaluate the emission performance, the emission current density J_A (=I_A/emission area) and the emission efficiency η (=I_A/I_C) were used.

Figure 2 shows the $J_A - V_G$ curves and the emission efficiency before and after ashing for all three types of GOS devices. Here, the applied voltage was restricted to near the onset voltage of electron emission to avoid a dielectric breakdown during emission measurement. Before ashing, the device without h-BN started to emit electrons at around V_G = 7 V, and the emission current density reached 1.02 mA/cm^2 with an emission efficiency of 17% at V_G = 8 V, as shown in Figure 2a. The device with multilayer h-BN was able to emit electrons even though the 13 nm thick h-BN layer was present in the emission area, as shown in Figure 2b. The emission current density reached 3.13 × 10^{-2} mA/cm^2, with an emission efficiency of 2.61 × 10^{-4}% at V_G = 11 V. However, the device required a slightly higher applied voltage of 10 V to start the emission and had a lower emission efficiency than the GOS without h-BN. This degradation of performance arose because some electrons emitted from the emission area were blocked by the thick h-BN layer and the organic residue on h-BN from the transfer process. The device with monolayer h-BN was also able to emit electrons, and the emission current density reached 1.25 mA/cm^2 at V_G = 9 V, as shown in Figure 2c. The emission efficiency reached 3% at V_G = 9 V and was lower than that of the GOS without h-BN. This result was also due to the organic residue on the transferred h-BN. By introducing a thinner h-BN layer instead of a 13 nm thick one, the emission current density and the emission efficiency were successfully improved.

After the first ashing for 4 min, the device without the h-BN protective layer was not able to emit electrons, indicating that the graphene electrodes were oxidized and removed because of the exposure to oxygen plasma, which was confirmed by the Raman spectrometry on the graphene electrode after ashing. The peak intensities of graphene were weakened after the ashing, as shown in Figure 3a, showing that most of the graphene electrode was oxidized and disappeared. In contrast, both devices with multilayer and monolayer h-BN succeeded in emitting electrons, as shown in Figure 2b,c. These results indicate that the graphene electrode underneath the h-BN remained under the oxygen plasma exposure, which is also supported by the Raman spectrometry results, as shown in Figure 3b,c. In addition, comparing these results with those before the ashing, the emission current density increased, and the emission efficiency improved. This is probably due to the removal of organic residue that had prevented the electron emission from the h-BN surface during ashing, considering the

https://doi.org/10.1021/acsomega.2c02709
ACS Omega 2022, 7, 33004−33009

electron emission efficiency of GOS devices was found to be improved due to the removal of the contamination of the surface of the GOS devices by the vacuum annealing in our previous study.[7] For the device with monolayer h-BN, the emission efficiency was increased to 11%, comparable to the GOS device without an h-BN protection layer. This result shows that a thin h-BN protective layer with a clean surface can provide oxygen tolerance to GOS devices without a significant emission loss. However, for some devices with monolayer h-BN, the emission performance deteriorates after ashing, probably because some oxygen intruded underneath the h-BN layer from small cracks and wrinkles in the transferred h-BN and partially oxidized the graphene electrode. Therefore, a smooth h-BN layer is ideally required to prevent oxygen intrusion under the h-BN and to further improve the device's oxygen resistance in future studies. One possible solution is the direct deposition of the h-BN layer onto the graphene electrode by CVD; h-BN with high crystallinity can be grown epitaxially on graphene because of the similar crystal structure of the two materials.[22]

After the second ashing for 4 min, the device with monolayer h-BN lost its capacity for electron emission. The monolayer h-BN was etched by oxygen plasma, resulting in oxidation and the loss of the graphene electrode, which was confirmed by Raman spectroscopy, as shown in Figure 3c. In contrast, the device with a thicker 13 nm h-BN layer was able to tolerate two ashing cycles, indicating that a thicker h-BN protective layer imparts more oxidation resistance to the GOS device; however, as seen from the results before ashing, the efficiency of the electron emission will deteriorate for devices with a thicker h-BN layer. Therefore, there is a trade-off between emission performance and oxygen resistance. Even though the GOS device was covered by multilayer h-BN, both the emission current density and the efficiency decreased after the second ashing. The cathode current of the device after the second ashing increased by one order of magnitude compared to that after the first ashing, and the cathode current density went from 4.6×10^4 to 3.3×10^5 mA/cm^2 when $V_G = 11$ V, indicating an increase in the leakage of current through the damaged SiO_2 layer. The GOS device is the capacitor structure with a very thin SiO_2 insulating layer with a thickness of around 10 nm. Therefore, the SiO_2 insulating layer was easily electrically damaged by static electricity. The SiO_2 layer has a soft breakdown by the charge up of the graphene electrode during an oxygen plasma exposure since the graphene electrode is electrically floated from the Si substrate. The voltage drop in the graphene electrode increased because of this leakage of current, and the effective applied voltage at the emission area was decreased. Therefore, the applied voltage required to initiate electron emission increased, and the $J_A - V_G$ curve became gradual, resulting in a decrease in the emission current density and the emission efficiency after the second ashing, as shown in Figure 2b,d. In addition, the Raman spectrometry analysis showed that the peak intensities of the graphene electrode with multilayer h-BN were not weakened after each ashing process, indicating that graphene was not damaged during ashing (see Figure 3b).

The thickness of multilayer h-BN was measured before and after ashing to investigate whether the h-BN is etched by the oxygen plasma treatment. A sample with a multilayer h-BN (13 nm)/SiO_2 (300 nm)/Si structure was prepared so that a square-shaped multilayer h-BN was fabricated by photolithography and reactive ion etching, as shown in Figure 4.

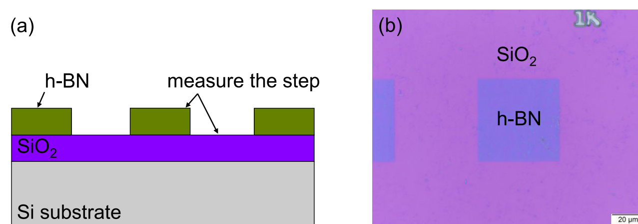

Figure 4. Sample with a multilayer h-BN/SiO_2/Si structure: (a) schematic and (b) optical image.

The distance between the tops of the h-BN and SiO_2 layers was measured by atomic force microscopy (AFM) before and after ashing to obtain the etched thickness of h-BN during the ashing process.

Three samples were prepared and exposed to oxygen plasma generated under the same conditions as in the device test for the times shown in Table 1. Samples 1 and 2 were exposed to air to measure the distance by AFM after the first ashing and then exposed to oxygen plasma again. For sample 3, ashing was performed twice in succession without exposure to air.

Table 1. Ashing Time for Three Samples

	ashing time (min)	
	ashing for the first time	re-ashing after exposure to air
sample 1	15	15
sample 2	30	30
sample 3	30 (15 min × 2 without exposure to air)	-

Figure 5 shows the amount of decrease in h-BN thickness with respect to total ashing time. The thickness reduction was calculated relative to the thickness of h-BN before ashing. The plots in the figure show the mean value of the h-BN thickness reduction, and the error bars show the standard error. For sample 1, the etched thickness reduction of h-BN after the first ashing was calculated to be negative, which appears to imply an increase in h-BN thickness; however, that cannot be the case. In addition, no deposition onto the surface of h-BN occurred under the experimental conditions, which was confirmed by the AFM image. Therefore, the negative etched thickness is

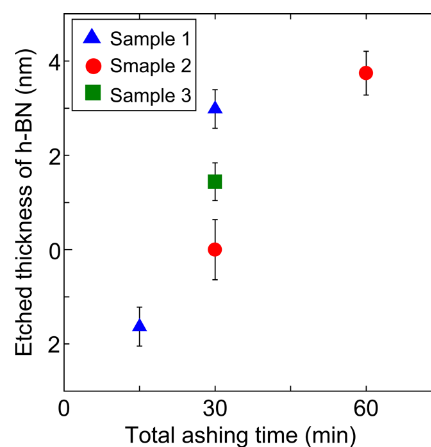

Figure 5. Decreasing amount of h-BN thickness with respect to total ashing time.

https://doi.org/10.1021/acsomega.2c02709
ACS Omega 2022, 7, 33004−33009

considered to be an artifact of the measurement, and the etched thickness of h-BN in sample 1 after the first ashing for 15 min is assumed to be negligible. Sample 2 was exposed to the oxygen plasma for 30 min for the first ashing; its etched thickness was also close to 0 nm. These results indicate that the etching of h-BN hardly progressed during the first ashing process. In contrast, although the ashing times of both the first and second ashing were the same, the etched thickness of both samples 1 and 2 after the second ashing exceeded 3 nm, indicating that the etching of h-BN occurred during the second ashing process. These results well correspond to the experimental results of oxygen resistance for the GOS devices with monolayer h-BN, as shown in Figure 3c. Namely, the h-BN layer can be etched by the second ashing process after the air exposure that follows the first ashing process.

One reason for the etching of h-BN to occur only after the second ashing process is the assistance of water in etching. In addition to oxygen, H_2O was likely to be present in the chamber for the ashing process because the inside of the process chamber was exposed to air when the sample was set, so that H_2O present in air adhered to the inner walls of the chamber and the sample surface. We hypothesize that this H_2O from the air contributed to the etching of h-BN. Previously, electron beam direct etching of h-BN using H_2O as a precursor gas has been reported, implying that chemisorbed H_2O contributed to the etching of h-BN.[23] In the first ashing, residual H_2O molecules are consumed in burning the thin layer of organic residue on the h-BN surface caused by the transfer process. Because the organic residue on the surface of h-BN had been removed in the first ashing, H_2O molecules are present to assist the etching of the h-BN layer in the second ashing.

To confirm our hypothesis for the effect of the residual H_2O molecules on h-BN etching during the ashing process, sample 3 was exposed to oxygen plasma for 15 min twice in succession without exposure to air except during the first sample set. Thus, at the start of the second ashing, virtually no organic residue or H_2O would exist on the sample surface because these species would have been removed during the first ashing. Therefore, by comparing the results of samples 1 and 3, the acceleration of h-BN etching during the ashing process by the H_2O on the h-BN surface can be confirmed. The total ashing time was equal for samples 1 and 3. However, the amount of h-BN etched in sample 1, which was exposed to air before the second ashing, is twice that of sample 3.

We further carried out additional experiments of the h-BN etching by air plasma, which contains H_2O molecules, to clarify the contribution of H_2O molecules to h-BN etching, as shown in Figure 6. To eliminate the effect of H_2O molecules adhered on the h-BN surface and the surface of the process chamber, the h-BN sample and the process chamber were annealed at 200 °C for 10 min under the base pressure of around 5×10^{-4} Pa. After cooling down to room temperature, h-BN sample was exposed to the air plasma (room temperature of 26 °C with a relative humidity of 45%) of 100 W with a pressure of 10 Pa. In the case of the air plasma etching of h-BN layer, etching of h-BN occurred at the first plasma treatment. In addition, the etched thickness of h-BN monotonically increased with respect to the total time of the air plasma treatment.

These results indicate that the H_2O directly adhering to the surface of h-BN accelerates the etching of h-BN during ashing. Therefore, at the second ashing of the GOS device with monolayer h-BN, the monolayer h-BN would be removed

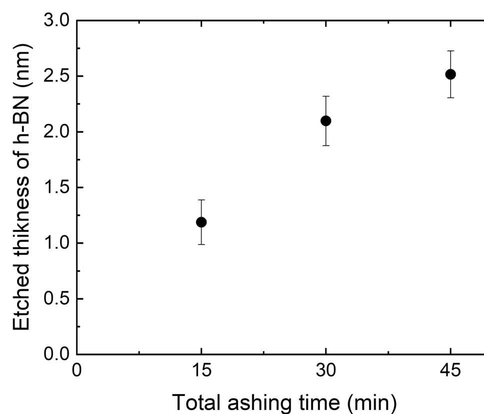

Figure 6. Etched thickness of h-BN by air plasma exposure as a function of total ashing time.

through this phenomenon, and the graphene electrode itself would be etched by the oxygen plasma, resulting in the loss of the device's emission capability.

■ CONCLUSIONS

In conclusion, by introducing h-BN as a protective layer on the graphene electrode of the GOS device, the oxidation resistance of the device was successfully improved while its emission performance was maintained. The device with monolayer h-BN tolerated oxygen plasma irradiation for 4 min and achieved an emission efficiency of 11%. A thicker h-BN layer imparted higher oxidation resistance to the device, but the emission efficiency decreased compared with the device with monolayer h-BN. Thus, there is a trade-off between the device's emission performance and its oxygen resistance. Therefore, the thickness of h-BN on the graphene electrode must be adjusted according to the requirements for the intended application of the device. We also found that oxygen plasma intruded through cracks and tears in the transferred h-BN, resulting in a partial etching of graphene and a decrease in its emission performance. Based on these findings, the direct deposit of h-BN on the GOS devices by CVD, which can provide smooth films with adjustable thickness, is an effective means of further improving the oxygen resistance of GOS devices as necessary for the desired applications. However, adherence of H_2O directly to the surface of h-BN is one probable cause of the acceleration of the etching of h-BN during ashing, resulting in the emission loss of the device with monolayer h-BN after the second ashing. For applications in liquid or air with H_2O, preventative measures must be followed to avoid the adherence of H_2O to the surface of h-BN, such as applying a hydrophobic treatment to the surface of h-BN.

■ AUTHOR INFORMATION

Corresponding Author

Katsuhisa Murakami − *National Institute of Advanced Industrial Science and Technology, Tsukuba 305-8568 Ibaraki, Japan*; orcid.org/0000-0001-5999-5581; Email: murakami.k@aist.go.jp

Authors

Naoyuki Matsumoto − *Department of Mechanical Engineering, Materials Science, and Ocean Engineering, Yokohama National University, Yokohama 240-8501,*

Japan; National Institute of Advanced Industrial Science and Technology, Tsukuba 305-8568 Ibaraki, Japan
Yoshinori Takao − *Division of Systems Research, Yokohama National University, Yokohama 240-8501, Japan*
Masayoshi Nagao − *National Institute of Advanced Industrial Science and Technology, Tsukuba 305-8568 Ibaraki, Japan*

Complete contact information is available at:
https://pubs.acs.org/10.1021/acsomega.2c02709

Notes

The authors declare no competing financial interest.

■ ACKNOWLEDGMENTS

This work was partly supported by JSPS KAKENHI Grant Numbers JP18H01505, JP18K18910, JP19K04516, and JP21H01401. This work has been done as part of JAXA/RDD's active space-debris removal research. A part of this work was conducted at the AIST Nano-Processing Facility supported by "Nanotechnology Platform Program" of the Ministry of Education, Culture, Sports, Science and Technology (MEXT), Japan. The authors thank Alicia Glatfelter, Ph.D., from Edanz (https://jp.edanz.com/ac) for editing a draft of this manuscript.

■ REFERENCES

(1) Kusunoki, T.; Suzuki, M.; Sasaki, S.; Yaguchi, T.; Aida, T. Fluctuation-Free Electron Emission from Non-Formed Metal-Insulator-Metal (MIM) Cathodes Fabricated by Low Current Anodic Oxidation. *Jpn. J. Appl. Phys.* **1993**, *32*, L1695−L1697.
(2) Shimawaki, H.; Neo, Y.; Mimura, H.; Murakami, K.; Wakaya, F.; Takai, M. Improvement of emission efficiency of nanocrystalline silicon planar cathodes. *J. Vac. Sci. Technol., B: Microelectron. Nanometer Struct.* **2008**, *26*, 864−867.
(3) Yokoo, K.; Tanaka, H.; Sato, S.; Murota, J.; Ono, S. Emission characteristics of metal−oxide−semiconductor electron tunneling cathode. *J. Vac. Sci. Technol., B: Microelectron. Nanometer Struct.* **1993**, *11*, 429−432.
(4) Ohta, T.; Kojima, A.; Koshida, N. Emission characteristics of nanocrystalline porous silicon ballistic cold cathode in atmospheric ambience. *J. Vac. Sci. Technol., B: Microelectron. Nanometer Struct.* **2007**, *25*, 524−527.
(5) Koshida, N.; Ohta, T.; Gelloz, B. Operation of nanosilicon ballistic electron emitter in liquid water and hydrogen generation effect. *Appl. Phys. Lett.* **2007**, *90*, No. 163505.
(6) Murakami, K.; Tanaka, S.; Miyashita, A.; Nagao, M.; Nemoto, Y.; Takeguchi, M.; Fujita, J. Graphene-oxide-semiconductor planar-type electron emission device. *Appl. Phys. Lett.* **2016**, *108*, No. 083506.
(7) Murakami, K.; Tanaka, S.; Iijima, T.; Nagao, M.; Nemoto, Y.; Takeguchi, M.; Yamada, Y.; Sasaki, M. Electron emission properties of graphene-oxide-semiconductor planar-type electron emission devices. *J. Vac. Sci. Technol., B: Nanotechnol. Microelectron.: Mater., Process., Meas., Phenom.* **2018**, *36*, No. 02C110.
(8) Murakami, K.; Miyaji, J.; Furuya, R.; Adachi, M.; Nagao, M.; Neo, Y.; Takao, Y.; Yamada, Y.; Sasaki, M.; Mimura, H. High-performance planar-type electron source based on a graphene-oxide-semiconductor structure. *Appl. Phys. Lett.* **2019**, *114*, No. 213501.
(9) Murakami, K.; Adachi, M.; Miyaji, J.; Furuya, R.; Nagao, M.; Yamada, Y.; Neo, Y.; Takao, Y.; Sasaki, M.; Mimura, H. Mechanism of Highly Efficient Electron Emission from a Graphene/Oxide/Semiconductor Structure. *ACS Appl. Electron. Mater.* **2020**, *2*, 2265−2273.
(10) Furuya, R.; Takao, Y.; Nagao, M.; Murakami, K. Low-power-consumption, high-current-density, and propellantless cathode using graphene-oxide-semiconductor structure array. *Acta Astronaut.* **2020**, *174*, 48−54.
(11) Miyaji, J.; Murakami, K.; Nagao, M.; Neo, Y.; Mimura, H. In *Evaluation of Electron Emission Properties of Graphene-oxide-silicon Planar Type Cold Cathode for an Electron Microscope*, 31st International Vacuum Nanoelectronics Conference (IVNC), Kyoto201812; IEEE, 2018.
(12) Kameda, Y.; Murakami, K.; Nagao, M.; Mimura, H.; Neo, Y. In *Microscope Equipped with Graphene-oxide-semiconductor Electron Source*, 34th International Vacuum Nanoelectronics Conference (IVNC), Lyon; IEEE, 2021; pp 1−2.
(13) Kimoto, Y.; Miyazaki, E.; Ishizawa, J.; Shimamura, H. Atomic Oxygen Effects on Space Materials in Low Earth Orbit and Its Ground Evaluation. *J. Vac. Soc. Jpn.* **2009**, *52*, 475−483.
(14) Li, L. H.; Cervenka, J.; Watanabe, K.; Taniguchi, T.; Chen, Y. Strong Oxidation Resistance of Atomically Thin Boron Nitride Nanosheets. *ACS Nano* **2014**, *8*, 1457−1462.
(15) Cheng, L.; Shi, Y.; Hao, Y.; Li, W.; Ren, S.; Wang, L. Multilayer boron nitride nanofilm as an effective barrier for atomic oxygen irradiation. *Appl. Surf. Sci.* **2020**, *504*, No. 144394.
(16) Liu, Z.; Gong, Y.; Zhou, W.; Ma, L.; Yu, J.; Idrobo, J. C.; Jung, J.; MacDonald, A. H.; Vajtai, R.; Lou, J.; Ajayan, P. M. Ultrathin high-temperature oxidation-resistant coatings of hexagonal boron nitride. *Nat. Commun.* **2013**, *4*, No. 2541.
(17) Li, X.; Yin, J.; Zhou, J.; Guo, W. Large area hexagonal boron nitride monolayer as efficient atomically thick insulating coating against friction and oxidation. *Nanotechnology* **2014**, *25*, No. 105701.
(18) Murakami, K.; Igari, T.; Mitsuishi, K.; Nagao, M.; Sasaki, M.; Yamada, Y. Highly Monochromatic Electron Emission from Graphene/Hexagonal Boron Nitride/Si Heterostructure. *ACS Appl. Mater. Interfaces* **2020**, *12*, 4061−4067.
(19) Igari, T.; Nagao, M.; Mitsuishi, K.; Sasaki, M.; Yamada, Y.; Murakami, K. Origin of Monochromatic Electron Emission From Planar-Type Graphene/h-BN/n-Si Devices. *Phys. Rev. Appl.* **2021**, *15*, No. 014044.
(20) Kern, W.; Puotinen, D. A. Cleaning Solutions Based on Hydrogen Peroxide for Use in Silicon Semiconductor Technology. *RCA Rev.* **1970**, *31*, 187−206.
(21) Kern, W. The Evolution of Silicon Wafer Cleaning Technology. *J. Electrochem. Soc.* **1990**, *137*, 1887−1892.
(22) Liu, Z.; Song, L.; Zhao, S.; Huang, J.; Ma, L.; Zhang, J.; Lou, J.; Ajayan, P. M. Direct Growth of Graphene/Hexagonal Boron Nitride Stacked Layers. *Nano Lett.* **2011**, *11*, 2032−2037.
(23) Elbadawi, C.; Tran, T. T.; Kolibal, M.; Sikola, T.; Scott, J.; Cai, Q.; Li, L. H.; Taniguchi, T.; Watanabe, K.; Toth, M.; Aharonovich, I.; Lobo, C. Electron beam directed etching of hexagonal boron nitride. *Nanoscale* **2016**, *8*, 16182−16186.